Master's Thesis

A Multiphase Lattice Boltzmann Model for Colloidal Particles and Surfactant in an Evaporating Droplet with a Pinned Contact Line

Jin Sol Choi

Department of Mechanical Engineering

Graduate School of UNIST

2019

A Multiphase Lattice Boltzmann Model for Colloidal Particles and Surfactant in an Evaporating Droplet with a Pinned Contact Line

Jin Sol Choi

Department of Mechanical Engineering

Graduate School of UNIST

A Multiphase Lattice Boltzmann Model for Colloidal Particles and Surfactant in an Evaporating Droplet with a Pinned Contact Line

A thesis/dissertation

submitted to the Graduate School of UNIST

in partial fulfillment of the

requirements for the degree of

Master of Science

Jin Sol Choi

December. 12. 2018

Approved by

Advisor

Chun Sang Yoo

A Multiphase Lattice Boltzmann Model for Colloidal Particles and Surfactant in an Evaporating Droplet with a Pinned Contact Line

Jin Sol Choi

This certifies that the thesis/dissertation of Jin Sol Choi is approved

12/Dec/2018

Signature

Advisor: Chun Sang Yoo

Signature

Hyungson Ki

Signature

Jaesung Jang

Abstract

When a colloidal droplet dries, a ring-shaped pattern remains along the droplet edge, which is referred to as the coffee-ring effect. Since this nonuniform deposition is undesirable in numerous practical applications in nanopatterning, many studies have attempted to attain uniform deposition patterns by altering the evaporation-induced flows with the aid of surfactant. Although the phenomenon seems simple, it is quite complex to model the deposition process of colloidal particles since multiple phases are involved in the system. A lattice Boltzmann method (LBM) has become a practical tool to simulate these complicated multiphase flows because of its simplicity in implementation. In this study, we develop a new lattice Boltzmann (LB) model to simulate evaporation of a droplet containing colloids and surfactant. The system is an isothermal system, where the evaporation is dominated by diffusion. The deposition process of colloidal particles is described by the macroscopic fluid model rather than a particle-based method to reduce the computation cost. That is, our model combines the pseudopotential LB model for evaporation of a droplet with the advection-diffusion LB model for colloids and surfactant. Here, we propose a new method to retain colloids and surfactant within the droplet during the phase change. The effect of surfactant on the surface flow is imposed by using Langmuir isotherm, which is one of the mostly used non-linear surfactant equations of state. We investigate the applicability of our model to generate the evaporation-induced velocity fields in a pinned droplet and to predict the contact angle evolution. These results match with the analytical solutions. Further, we obtain the deposition patterns of colloids at the contact line by varying Peclet numbers. Finally, we show the unique behaviors of the drying droplet containing surfactant, such as the pinning-depinning contact line dynamics, and the inflation and deflation at the droplet center and at the edge, respectively.

Contents

List of Figures

List of Tables

1 Introduction

1.1. Physical background

When a spilled coffee dries, a ring-shaped pattern remains along the droplet edge, which is commonly referred to as the coffee-ring effect [1]. Since this phenomenon is undesirable in many industrial fields, such as coating [2], nanoassembly [3], nanopatterning [4], and inkjet printing [5], strategies for controlling deposition patterns are needed based on comprehension of the mechanisms for the droplet evaporation and the deposition process.

The deposition pattern of the particle is largely affected by evaporation. There are two different modes of evaporation: one is the constant radius (CR) mode and the other is the constant angle (CA) mode [6]. In the CR mode, the contact angle of an evaporating droplet deceases with constant contact radius. In the CA mode, the droplet maintains a certain contact angle and the contact radius recedes during the evaporation. In reality, the evaporation of a droplet shows the combined mode of CR and CA, called the "stick-slip" mode [7, 8] because of irregular roughness [9-11] or chemical inhomogeneity [12-14] of the substrate. During this combined mode, the droplet initially evaporates in the CR mode and then changes its mode to the CA mode when the balance of Young's force is broken. In a droplet evaporating in the CR mode, colloidal particles are delivered to the droplet edge due to the outward capillary flow [15] and are accumulated in the vicinity of the droplet edge forming the coffee-ring pattern. If the depinning occurs, the contact line recedes pulling the accumulated particles toward the center of a droplet, leaving the final dot-like pattern at the center.

The flow field in an evaporating droplet has been studied since the flow affects the behavior and deposition pattern of particles. In particular, the pioneering study of Deegan et al. [1] elucidated that the outward capillary flow attributes to the coffee-ring effect of the droplet. Hu and Larson [16, 17] numerically studied the effect of temperature gradient on the droplet surface on the velocity field, and concluded that the coffee ring pattern forms due to both the fixed contact line and the suppression of the counteracting flow. The counteracting flow is commonly referred to as the Marangoni flow that is generated by either temperature gradient or concentration gradient at the liquid interface. Marin et al. [18] experimentally investigated the effect of surfactant on the flow inside a droplet induced by evaporation.

However, few have visualized and quantitatively measured the flow field in an evaporating droplet to predict the final deposition pattern. Due to such limitations of the experimental study, many studies are trying to obtain the flow field either numerically or analytically. Maki and Kumar [19] solved the full convection-diffusion equation of colloid particles by applying the lubrication approximation and elucidated the skin formation by capturing the depth-wise gradient of particle concentration. For numerical studies, Zhao and Yong [20] developed a free-energy-based multiphase lattice Boltzmann

model to simulate the evaporation of the colloidal droplet on a solid surface with specified wetting properties. Frijters et al. [21] applied the amphiphile LB model to investigate the effect of surfactant and compared it with the effect of colloids on droplets in the presence of shear flow. Despite the numerical and theoretical studies for the particle-laden droplet evaporation, a unified method within the LBM to predict the velocity field and the behaviors of colloids and surfactant has not been developed.

1.2. The lattice Boltzmann method

The motion of fluid can be described by three ways according to the observed scales; continuum models at the macroscopic scale, kinetic theories at the mesoscopic scale, and microscopic models at molecular scale as illustrated in Fig. 1.

In the continuum approach, governing equations are obtained by applying the conservation laws of mass, momentum, and energy to a control volume of fluid. Nonetheless, these equations are difficult to solve since the equations are usually highly nonlinear. A clever breakthrough for this problem is to convert the equations into a system of algebraic equations by using finite difference, finite volume, and finite element schemes and solve the system of equations numerically.

In microscopic models, such as molecular dynamics (MD) simulation, the movements of individual molecules are simulated based on the Newtonian equation. This MD simulation has received attention with increasing interests in micro and nanoscale technology. However, the simulation requires a huge amount of computational cost as the simulation domain increases.

The mesoscopic models are proposed to relate the microscopic and macroscopic scales of the simulations. As one of the mesoscopic models, the lattice Boltzmann method (LBM) has drawn great attention due to its advantages. Differing from MD, which considers the individual behavior of particles, LBM simulates the motion of fluid by considering the distribution of particles. The collection of particles is expressed by the distribution function that is governed by the Boltzmann equation. Due to its kinetic nature, it is feasible to implement complex geometries and parallel computing in the LBM. In addition, the LBM is an appropriate way to simulate multiphase and multicomponent flows without a need of capturing the interface between two different phases.

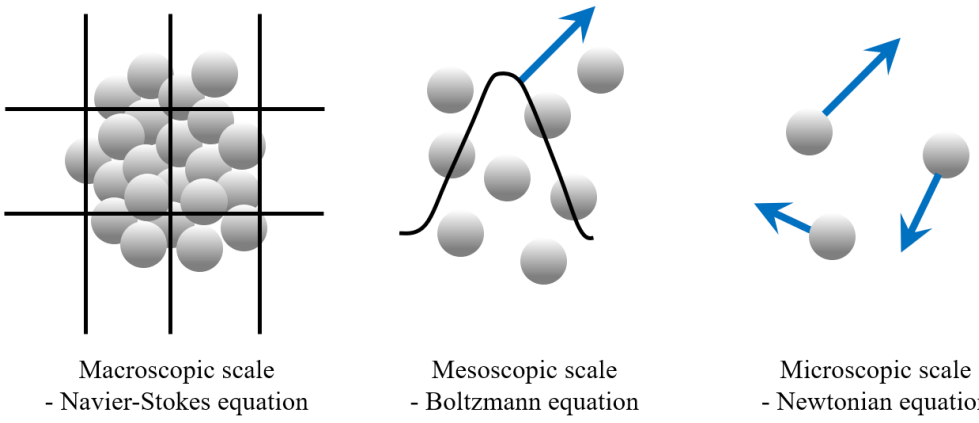

Figure 1. Schematic of various simulation scales: macroscopic, mesoscopic, and microscopic scale.

The pseudopotential lattice Boltzmann model, also called as Shan-Chen (SC) model, is proposed by Shan and Chen in 1993 [22] to simulate the multiphase flows with LB method. In the model, phase separation occurs by imposing the interaction force between particles that allows for a non-ideal gas behavior of fluids. This is one of the most popular models for multiphase flows because of its simplicity in implementation and adaptability in complex geometries. Despite the advantages, the original SC model has several limitations that:

1. it cannot simulate a problem that has large density ratio between the two phases,
2. meaningful velocity field can rarely be obtained due to the presence of the spurious current caused by the imbalance between discretized pressures near the interface, and
3. it cannot specify the surface tension independently to the model.

To resolve such problems of the SC model, many studies have been conducted in the past few decades. Zhu et al. [23] introduced a pseudopotential model to simulate large density ratio of fluids by including multiple-relaxation-time (MRT) scheme with the Carnahan-Starling equation of state. Shan [24] proposed a method to reduce spurious current by incorporating more neighbors when calculating the interaction force which leads to a higher order of isotropy.

1.3. Objective

The objective of this research is to develop a new lattice Boltzmann (LB) model to simulate the evaporation of a droplet containing colloids and surfactant. Our model consists of the pseudopotential LB model for the evaporation of a droplet and the advection-diffusion LB model for colloids and surfactant. Here, we propose a new approach to retain colloids and surfactant within the droplet during the phase change of a droplet caused by solvent evaporation. The effect of surfactant on the surface tension is also incorporated in the model by using the Langmuir's isotherm that is one of the mostly used non-linear surfactant equations of state.

Our simulation results are three-fold: (1) the velocity fields inside the droplet and the contact angle evolution are achieved and are compared with analytic solutions, (2) the deposition patterns are investigated by varying the Peclet numbers, and (3) the contact line dynamics and the inflation of the droplet shape caused by the Marangoni flow are obtained.

2. Simulation model

2.1. The lattice Boltzmann model for simulating multiphase flows

The basic idea of LBM is to treat a statistical group of fluid particles as fictitious particles. By discretizing the following Boltzmann equation with BGK operator,

$$\frac{\partial f}{\partial t} + c \cdot \nabla f = \frac{1}{\tau}(f^{eq} - f) \tag{2.1}$$

we obtain the lattice Boltzmann equation (LBE):

$$f_i(x + c_i\Delta t, t + \Delta t) = f_i(x,t) + \frac{1}{\tau}(f_i^{eq}(x,t) - f_i(x,t)). \tag{2.2}$$

The equation describes the movement of particles f_i toward the neighboring node $x + c_i\Delta t$ with velocity c_i, where c_i is a discrete set of velocities, Δt is the time step, and f_i is the distribution function evolving with time in the c_i direction. Simultaneously, particles are affected by the collision operator term in the RHS of Eq. (2.1) and redistributed. These two processes are called collision and streaming processes, respectively, as illustrated in Fig. 2.

The collision operator term expresses the relaxation of distribution function f_i to the equilibrium distribution function f_i^{eq} by the single relaxation time, τ. The equilibrium distribution function is given by

$$f_i^{eq}(x,t) = w_i\rho\left(1 + \frac{u \cdot c_i}{c_s^2} + \frac{(u \cdot c_i)^2}{2c_s^4} - \frac{u \cdot u}{2c_s^2}\right) \tag{2.3}$$

where c_s is the sound of speed and w_i is the weight determined by the speed sets. Qian et al. [25] proposed the DnQm models of the speed sets, where n represents the dimension of the domain, and m refers to the number of velocities in the sets. The common speed model for the fluid problem is D2Q9 (2-dimension & 9 velocities), where $c_s = 1/\sqrt{3}$, $c_i = \{(0,0), (\pm1,0), (0,\pm1), (\pm1,\pm1)\}$, $w_0 = 4/9$, $w_{1\sim4} = 1/9$, and $w_{5\sim8} = 1/36$. By choosing the equilibrium function, we can obtain the macroscopic variables since the equilibrium distribution function enforces the mass and momentum conservation during the collision process:

$$\sum_i f_i^{eq} = \sum_i f_i = \rho\,, \qquad \sum_i c_i f_i^{eq} = \sum_i c_i f_i = \rho u. \tag{2.4}$$

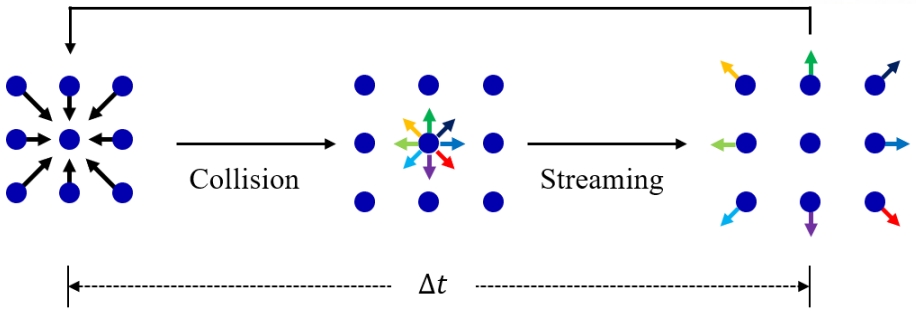

Figure 2. The schematic of collision and streaming process in the D2Q9 lattice Boltzmann

For multicomponent fluids consisting of N species, the evolution equation of each component can be written as

$$f_i^k(x + c_i\Delta t, t + \Delta t) = f_i^k(x,t) + \frac{1}{\tau}\left(f_i^{k,eq}(x,t) - f_i^k(x,t)\right), \qquad k = 1, \cdots, N \tag{2.5}$$

where the equilibrium distribution function is as follows:

$$f_i^{k,eq}(\rho^k, u_{eq}^k) = w_i\rho^k\left(1 + \frac{1}{c_s^2}(c_i \cdot u_{eq}^k) + \frac{1}{2c_s^2}(c_i \cdot u_{eq}^k)^2 - \frac{1}{2c_s^2}u^{k\,2}_{eq}\right). \tag{2.6}$$

The macroscopic densities and velocities are defined as follows:

$$\rho^k = \sum_i f_i^k, \tag{2.7}$$

$$u^k = \frac{1}{\rho^k}\sum_i c_i f_i^k. \tag{2.8}$$

We can model multicomponent systems postulating interaction forces in the LBM. Shan and Chen incorporated the interaction force between particles to make the fluid immiscible.

$$F^k(x,t) = -G^{k\bar{k}}\psi^k(x,t)\sum_{i=1}^{8} w_i\psi^{\bar{k}}(x + c_i\Delta t, t)c_i. \tag{2.9}$$

The force includes the interaction between two fluid components at the nearest neighbor and the sign of parameter, $G^{k\bar{k}}$, determines whether the interaction force is attraction (when negative) or repulsion (when positive). In the multicomponent multiphase model, positive $G^{k\bar{k}}$ should be chosen to make a separation between the components. After equilibration, a denser phase of density ρ_{ma}^k and a lighter phase of density ρ_{mi}^k is formed at each component. In this thesis, ψ^k, the effective mass, is defined as

$$\psi^k(x,t) \equiv \psi\left(\rho^k(x,t)\right) = 1 - e^{-\rho^k(x,t)}. \tag{2.10}$$

To include the interaction force to LBM, Shan and Chen introduced the equilibrium velocity u_{eq}^k

$$u_{eq}^k(x,t) = u_{bulk}(x,t) + \frac{\tau^k F^k(x,t)}{\rho^k(x,t)}, \tag{2.11}$$

where u_{bulk} is the macroscopic velocity of the bulk fluid:

$$u_{bulk} = \frac{\sum_k \sum_i c_i f_i^k}{\sum_k \sum_i f_i^k}. \tag{2.12}$$

Since the interaction force F^k is imposed, the local momentum is not conserved before and after collision [26]. Therefore, the macroscopic fluid velocity which expresses the motion of the fluid is defined by averaging momenta before and after the collision step:

$$\rho U_f = \sum_k \sum_i c_i f_i^k + \frac{1}{2} \sum_k F^k, \tag{2.13}$$

where ρ is the sum of densities from each component.

In the next section, we introduce LB models developed for simulating the evaporation of a colloidal droplet containing surfactant within the frame work of the pseudopotential lattice Boltzmann method: (i) models for the evaporation of a droplet and for the pinning of a droplet contact line, respectively, (ii) a model for the droplet of a colloidal solution combined with the advection-diffusion LB method [27-29], and (iii) a model for the surface tension force induced by surfactant. Here, we assume the system is isothermal and the evaporation occurs by the density gradient of the fluid surrounding the droplet. Special attention is paid in combining the two-component pseudopotential LB model for a drying droplet with the one-component advection-diffusion LB method for the colloidal solution to simulate a drying colloidal droplet. More details are provided in the section 2.3.

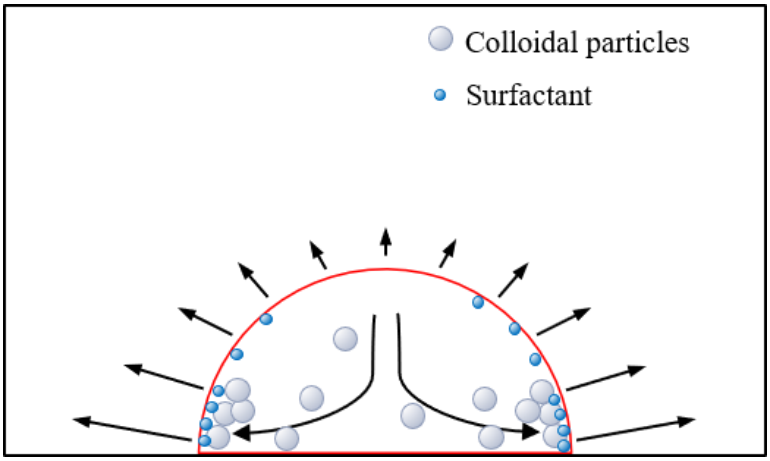

Figure 3. Schematic of the evaporation of a droplet containing colloidal particles and surfactant.

2.2. Models for the evaporation of a droplet and a pinned contact line

The evaporation is successfully depicted by implementing the evaporation model of Hessling et al. [30] which focuses on the two-component version of the pseudopotential lattice Boltzmann method. The main idea of this model is to form a density gradient in the vapor phase of the droplet by setting a constant density lower than ρ_{mi}^{σ} at the domain boundaries. This density gradient surrounding the droplet induces diffusion of fluid component σ toward the minimum. Suppose the evaporation boundary is located on x_H in the domain, then the density at this site is set to be a constant value of $\rho(x_H, t) = \rho_H^{\sigma}$ by the following distribution function

$$f_i^{\sigma}(x_H, t) = f_i^{eq}\left(\rho_H^{\sigma}, u_H^{\sigma}(x_H, t)\right), \tag{2.14}$$

where $u_H^{\sigma}(x_H, t) = 0$, which ensures an undisturbed flow field in the system. Furthermore, we set the density of $\rho^{\bar{\sigma}}$ as Eq. (2.15) to retain total mass conservation within the simulation domain

$$\rho^{\bar{\sigma}}(x_H, t) = \rho^{\sigma}(x_H, t-1) + \rho^{\bar{\sigma}}(x_H, t-1) - \rho_H^{\sigma}, \tag{2.15}$$

also set the velocity as

$$f_i^{\bar{\sigma}}(x_H, t) = f_i^{eq}\left(\rho_H^{\bar{\sigma}}, u_H^{\bar{\sigma}}(x_H, t)\right). \tag{2.16}$$

To fix the contact line of the droplet during evaporation, we generate unbalanced Young's force by using hydrophobic and hydrophilic substrate. The mechanism of this pinning phenomenon is reported in several studies [13]. Li et al. [14] performed a hybrid thermal multiphase lattice Boltzmann simulation for the evaporating droplet on a chemically patterned substrate. In the study, they numerically solved the temperature equation and coupled the temperature field with the fluid flow through the Peng-Robinson equation of state [31] to simulate evaporation. They observed "stick-slip-jump" behavior of an evaporating droplet and illustrated that the contact line is fixed by adjusting the fraction of contact lines occupied by each component on the patterned substrate. Therefore, we applied the unbalanced Young's force to fix the contact line by locating the droplet on the hydrophilic substrate (A) and setting surrounding as hydrophobic substrate (B) as demonstrated in Fig. 4. In the figure, the unbalanced Young's force at each substrate is defined as follows:

$$F_{u,A} = \gamma(\cos\theta - \cos\theta_A), \qquad F_{u,B} = \gamma(\cos\theta - \cos\theta_B), \tag{2.17}$$

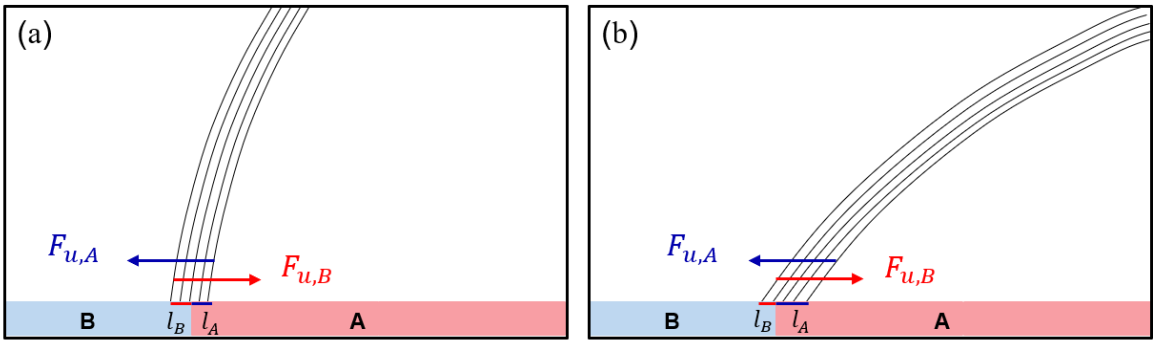

Figure 4. Young's force after equilibration (a) and during evaporation (b). The substrates A and B indicate hydrophilic and hydrophobic substrate respectively. The equal length fractions of l_B and l_A at equilibrium (the red and blue lines, respectively) are changing during evaporation.

where γ denotes liquid-gas surface tension, θ_A and θ_B are equilibrium contact angle at each substrate, and θ is measured contact angle. At equilibrium, the two unbalanced Young's forces are locally balanced retaining the contact line to be fixed. As a result, the horizontal force balance can be written as:

$$\gamma l_A(\cos\theta - \cos\theta_A) = \gamma l_B(\cos\theta - \cos\theta_B). \tag{2.18}$$

Note that the diffusion interface between two different phases exists in the pseudopotential model, the forces are proportional to the length fraction of the contact area of the interface, which is denoted be l_A and l_B. After equilibration, the contact angle is $\theta \approx 90^\circ$ and the length fraction l_A and l_B are almost equally distributed. As evaporation proceeds, $F_{u,A}$ decreases as $|\cos\theta - \cos\theta_A|$ decreases. Consequently, the length fraction l_A occupied by substrate A increases to maintain the force balance in Eq.(2.18) as illustrated in Fig. 4b.

To implement the hydrophobic and hydrophilic boundary conditions, we incorporate forces between two fluids, σ and $\bar{\sigma}$, and solid substrate [32]. The interaction force is given as

$$F_{ads}^{k}(x,t) = -G_{ads}^{k}\psi^{k}(x,t)\sum_{i=1}^{8} w_i s(x + e_i\Delta t, t)e_i\,, \qquad k = \sigma, \bar{\sigma} \tag{2.19}$$

where $s = 0$ or 1 for a fluid node or a solid node, respectively. The sign of the adhesion interaction parameter G_{ads}^{k} determines the fluid wettability on the substrate (positive for hydrophobic substrate and negative for hydrophilic substrate) and the magnitude of G_{ads}^{k} specifies the contact angle. The contact angle is defined at the point where the fluid-fluid and the fluid-solid interfaces meet. The relationship between the contact angle and the interfacial tension is defined by Young's equation:

$$cos\theta_\sigma = \frac{\gamma_{\sigma s} - \gamma_{\bar{\sigma} s}}{\gamma_{\sigma\bar{\sigma}}}, \tag{2.20}$$

where $\gamma_{\sigma s}$ and $\gamma_{\bar{\sigma} s}$ are the interfacial tension between each fluid component (σ and $\bar{\sigma}$) and the substrate, and $\gamma_{\sigma\bar{\sigma}}$ is the interfacial tension between two fluid components. Huang et al. [33] suggested a straightforward implementation of the Young's equation to the LBM by using the relationship (Eq. (2.21)) between the adhesion parameters G_{ads}^{k} of each fluid component and the substrate with a density factor $(\rho_{ma}^{\sigma} - \rho_{ma}^{\bar{\sigma}})/2$.

$$cos\theta_\sigma = \frac{G_{ads}^{\bar{\sigma}} - G_{ads}^{\sigma}}{G\dfrac{\rho_{ma}^{\sigma} - \rho_{ma}^{\bar{\sigma}}}{2}}. \tag{2.21}$$

By varying G_{ads}^{k}, various contact angles are obtained at the same initial condition as shown in Fig. 5.

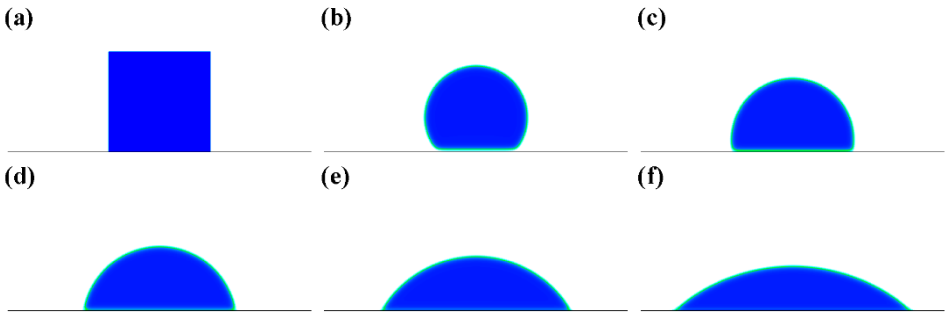

Figure 5. (a) an initial condition used in the simulations. The density of each fluid component σ is given in $60 \times 60\ \mathrm{lu}^2$ sized blue square of the fluid σ surrounded by $\bar{\sigma}$. The total simulation domain is $181 \times 73\ \mathrm{lu}^2$. (b)-(f) Various contact angles are obtained using different values of the interaction parameter G_{ads}^{k} between fluid components and the solid substrate. The specific values of the parameters and the measured contact angles are listed in Table 1.

Table 1. Adhesion parameters and contact angles

Case	G_{ads}^{k}	Contact angle calculated from Eq (2.21)	Contact angle measured from Figure 5
b	0.2089	130°	128.5°
c	0.0564	100°	99.5°
d	-0.0564	80°	84.4°
e	-0.1625	60°	70°
f	-0.2489	40°	54°

2.3. Models for colloidal particles and surfactant

In this section, we will introduce an LB method to obtain the particle concentration dissolved in an evaporating droplet. To model the particle concentration in a continuum level, we assume that the particle diameter is much smaller than the height of the droplet. Based on the assumption, the particle concentration, c, is governed by the advection-diffusion equation. We solve the equation using the LBM. Note that the lattice Boltzmann equation for the shape evolution of a drying droplet will be solved separately prior to solving the advection-diffusion equation.

2.3.1. Model for colloidal particles

The concentration of colloidal particles in a single-phase flow can be simulated by the method proposed by Michalis et al. [29]. In the model, the evolution of colloid particle concentration can be depicted by the following LB equation.

$$f_i^c\left(x + e_{c,i}\Delta t, t + \Delta \mathrm{t}\right) = f_i^c(x,t) - \frac{1}{\tau^c}\left(f_i^c - f_i^{eq}\right), \qquad \mathrm{i} = 0, \cdots, 8. \tag{2.22}$$

The macroscopic density and the velocity can be recovered by their momentums:

$$\rho^c(\mathrm{x},\mathrm{t}) = \sum_i f_i^c(x,t) = \sum_i f_i^{eq}(x,t), \tag{2.23}$$

$$\rho^c \boldsymbol{v}(\mathrm{x},\mathrm{t}) = \sum_i f_i^c(x,t)c_i = \sum_i f_i^{eq}(x,t)c_i, \tag{2.24}$$

where the equilibrium distribution function of the colloid particles can be expressed by the density ratio of the colloid particle (ρ^c) and the fluid (ρ^σ) as follows [27]:

$$f_i^{c,eq} = \left(\frac{\rho^c}{\rho^\sigma}\right) f_i^{\sigma,eq}(\rho^\sigma, \boldsymbol{v}). \tag{2.25}$$

The distinctive feature of the LB method for the advection-diffusion equation compare to Navier-Stokes equation is that the velocity, $\boldsymbol{v}$, used in computing $f_i^{\sigma,eq}$ is externally obtained rather than calculated from its distribution function: we obtain $\boldsymbol{v}$ from the velocity of the medium fluid (solvent).

Through the Chapman-Enskog expansion, the following advection-diffusion equation can be recovered.

$$\frac{\partial \rho^c}{\partial t} + \nabla \cdot (\rho^c \boldsymbol{v}) - D_c \nabla^2 \rho^c = 0. \tag{2.26}$$

The diffusion coefficient of the colloid particle D_c is calculated by

$$D_c = c_s^2\left(\tau^c - \frac{1}{2}\right), \tag{2.27}$$

where $c_s^2 = 1/3$ and τ^c is the relaxation of the colloid particle.

Applying this equation to the multiphase flow, let the shared velocity between the colloid particle and the fluid be U_f, which is calculated as the average of the momenta before and after collisions in Eq. (2.13). Therefore, the equilibrium distribution function of the particle concentration dissolved in the multiphase flow becomes

$$f_i^{c,eq} = w_i\rho^c\left(1 + \frac{1}{c_s^2}(c_i \cdot U_f) + \frac{1}{2c_s^2}(c_i \cdot U_f)^2 - \frac{1}{2c_s^2}U_f^2\right), \tag{2.28}$$

which recovers the advection-diffusion equation through Chapman-Enskog expansion:

$$\frac{\partial\rho^c}{\partial t} + \nabla\cdot(\rho^c U_f) - D_c\nabla^2\rho^c = 0. \tag{2.29}$$

The bulk fluid velocity U_f is obtained at all grid points in the total simulation domain. Thus, we impose the external force to retain particles in the droplet. The force term is similar to the Shan-Chen interaction force, F_{int}, where G_{int} is the coefficient of the interaction force.

$$F_{int}(x,t) = -G_{int}\psi^c(x,t)\sum_{i=1}^{8} w_i\psi^\sigma(x + e_i\Delta t, t)e_i. \tag{2.30}$$

The external force is applied by modifying the fluid velocity U^f:

$$u_{eq}^c = U^f + \frac{\tau^c}{\rho^c}F_{int}. \tag{2.31}$$

The equilibrium distribution function with the modified velocity u_{eq}^c can be expressed as follows:

$$f_i^{c,eq} = w_i\rho^c\left(1 + \frac{1}{c_s^2}(c_i \cdot u_{eq}^c) + \frac{1}{2c_s^2}(c_i \cdot u_{eq}^c)^2 - \frac{1}{2c_s^2}u^{c2}_{eq}\right). \tag{2.32}$$

Since the momenta before and after the collisions are not conserved in this forcing scheme [34], the bulk velocity of the particles U^c can be obtained by averaging the momentums before and after the

collisions:

$$U^c = U^f + \frac{\tau_c}{2\rho^c} F_{int}. \tag{2.33}$$

2.3.2. Model for surfactant

The property of the surfactant is different from the colloid particles in that they have the propensity to absorb at the surface of a droplet. When they are absorbed in the surface, the surface free energy is reduced which results in a reduction of surface tension of the droplet. To simulate the behavior of the surfactants, we modified the model of colloidal particle introduced in Section 2.3.1. In this model, we introduce the surfactant-induced surface tension of a droplet by using the Langmuir isotherm, which is one of the mostly used non-linear surfactant equations of state [35]. The equation is based on a lattice-type model and assumes that:

1. there are no intermolecular forces between surfactant molecules;
2. all the adsorption site on the lattice is tantamount; and
3. the tendency to absorb at an empty site has no relevance to the occupancy of neighboring sites.

The formulation is expressed as follows:

$$\sigma = \sigma_0 + RT\Gamma_\infty \ln\left(1 - \frac{\Gamma}{\Gamma_\infty}\right), \tag{2.34}$$

where σ is the surface tension, σ_0 is the surface tension of the pure solvent, and Γ_∞ is the saturation surfactant concentration. Here, the product of the universal gas constant and the temperature, RT, is fixed as 1/3 for an isothermal pseudopotential lattice Boltzmann model. Based on the surfactant equation of state, we can obtain the net force induced by the presence of the surfactant concentration gradient at each lattice site:

$$F_{net} = A_0(\nabla \cdot \sigma), \tag{2.35}$$

where A_0 is the area of each lattice. The surfactant concentration gradient on the droplet surface induces force, F_{net}, which is imposed by adding the net force to the equilibrium velocity, u_{eq}^{σ}, of the medium fluid in Eq. (2.11). Then, we obtain the modified equilibrium velocity $u_{eq,mod}^{\sigma}$ for the fluid component σ of the medium fluid:

$$u^{\sigma}_{eq,mod} = u^{\sigma}_{eq} + \frac{\tau^{\sigma}}{\rho^{\sigma}} F_{net}. \tag{2.36}$$

The concentration of the surfactant is obtained by the model proposed in Section 2.3.1. The Chapman-Enskog analysis of the proposed model to simulate the surfactant induced flows will remain as a future work.

2.4. Simulation algorithm

The algorithm of the simulation is shown in Fig. 6.

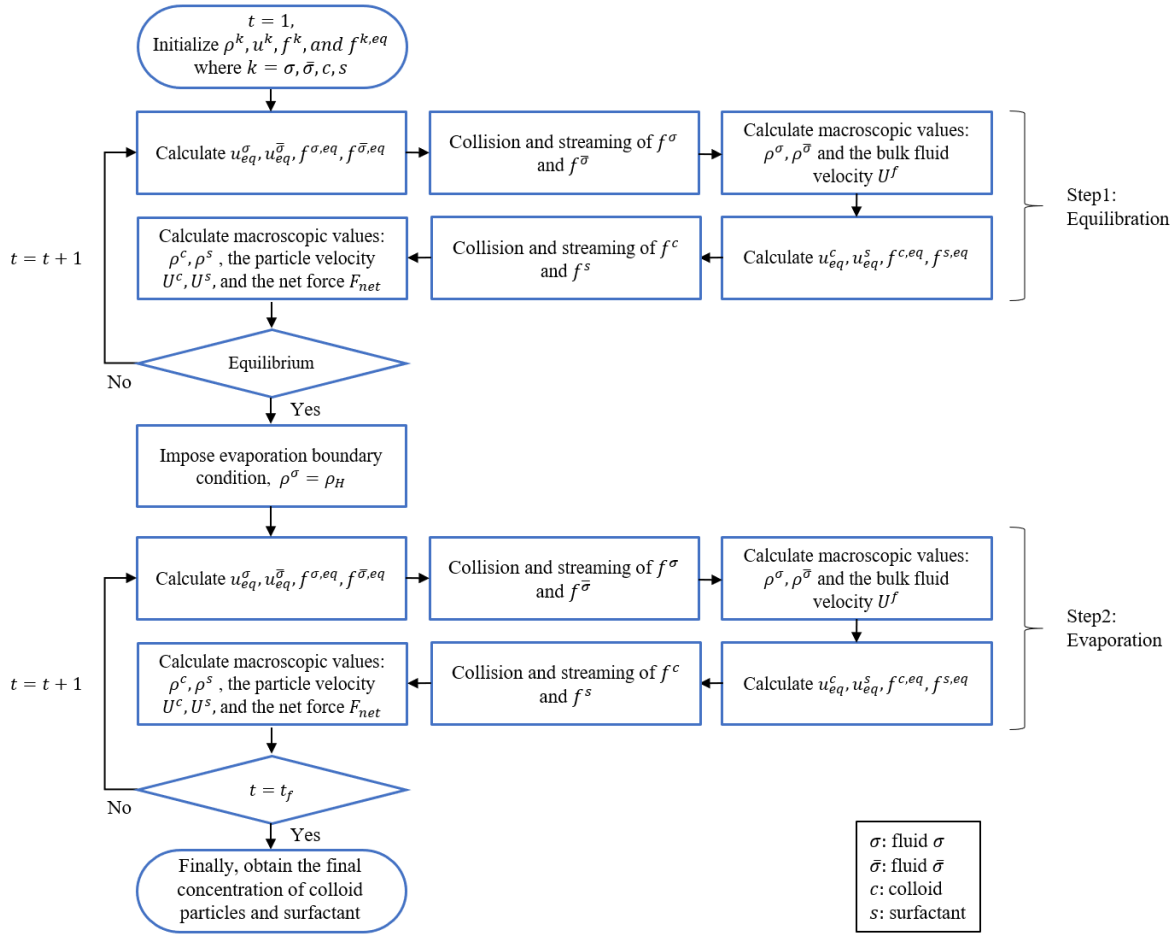

Figure 6. Simulation algorithm

3. Simulation results and discussion

3.1. Evaporation of a droplet with a pinned contact line

We first simulate the evaporation of a pure droplet with a pinned contact line using our newly developed LB model. The simulation is conducted in a 3-dimensional domain, size of $101 \times 101 \times 51$. The boundary conditions except for the bottom substrate are periodic during equilibration. The substrate is chemically patterned, where the hydrophilic ($\theta_A \approx 0^\circ$) circle is imposed at the center of the simulation domain and surrounded by hydrophobic ($\theta_B \approx 130^\circ$) area, as illustrated in Fig. 7. The initial conditions of the droplet are set to be the contact radius of $R_0 = 40$ with the initial contact angle of $\theta_0 \approx 90^\circ$, and the densities of $\rho_{ma}^{\sigma} = \rho_{mi}^{\bar{\sigma}} = 0.7$ and $\rho_{mi}^{\sigma} = \rho_{ma}^{\bar{\sigma}} = 0.04$. The interaction parameter in Eq. (2.19) is set to $G_{\sigma\bar{\sigma}} = 2.8$.

After equilibration, we obtain the equilibrium densities of $\rho_{ma}^{\sigma} \approx 0.64$ and $\rho_{mi}^{\sigma} \approx 0.12$. Then we run the simulation for the evaporation of the droplet. For this, we imposed $\rho_H = 0$ at all sides of the computation domain except the bottom where the wall boundary condition is imposed.

By assuming that the evaporation of the droplet is in a quasi-steady state and dominated by the density gradient of the surrounding fluid, the surrounding fluid density ρ^{σ} satisfies the Laplace equation,

$$\Delta\rho^{\sigma} = 0, \tag{3.1}$$

with the boundary conditions that the vapor is saturated at the constant concentration of $\rho^{\sigma} = \rho_H$. Since this boundary value problem is mathematically equivalent to the electrostatic problem of a charged conductor, several researchers derived the formulas and solved for ρ^{σ}. Stauber et al. [36] derived an equation describing the contact angle evolution of the droplet which evaporates in the constant contact radius mode,

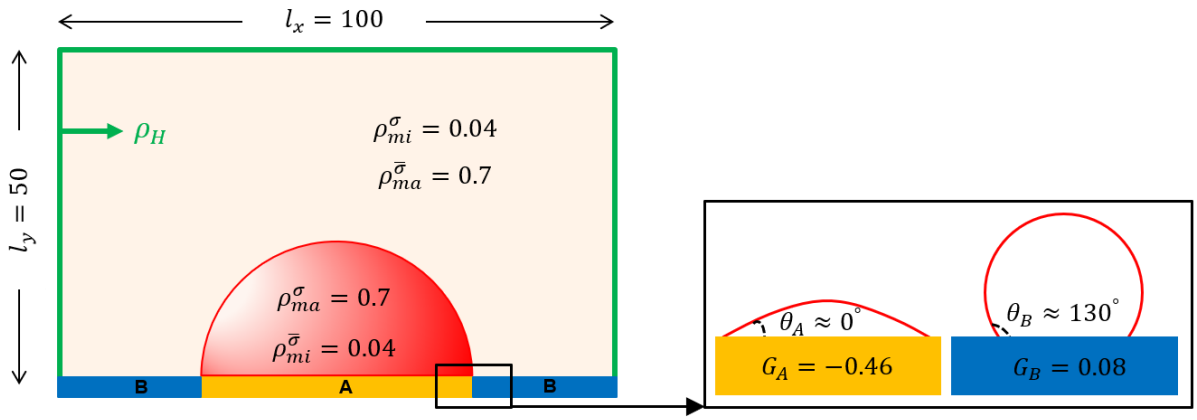

Figure 7. Schematic of the simulation domain

$$\frac{d\theta}{dt} = -\frac{D(\rho_{mi}^{\sigma} - \rho_H)}{\rho_{ma}^{\sigma} R_0^2} g(\theta), \tag{3.2}$$

where the function $g = g(\theta)$ is defined by:

$$g(\theta) = (1 + cos\theta)^2 \left\{ tan\frac{\theta}{2} + 8\int_0^{\infty} \frac{\cosh^2 \theta\tau}{\sinh 2\pi\tau} \tanh[\tau(\pi - \theta)] d\tau \right\}. \tag{3.3}$$

To apply this equation to the multicomponent pseudopotential model, we use the diffusion coefficient D is given as [30]:

$$D = \left[c_s^2 \left(\tau^{\sigma} - \frac{1}{2} \right) - \frac{c_s^2}{\rho^{\sigma} + \rho^{\bar{\sigma}}} (\rho^{\bar{\sigma}} \psi^{\sigma} G^{\sigma\bar{\sigma}} \psi'^{\bar{\sigma}} + \rho^{\sigma} \psi^{\bar{\sigma}} G^{\bar{\sigma}\sigma} \psi'^{\sigma}) \right]. \tag{3.4}$$

We numerically solve Eq. (3.2) with 4th-order Runge-Kutta method for the contact angle θ. Fig. 8 compares the evolution of contact angle θ in the droplet evaporating in CR mode versus the normalized time t/t_f where t_f is the lifetime of the droplet when the contact angle becomes zero. The solid line indicates the analytic solution obtained by Eq. (3.2) and the symbols correspond to the results of LB simulation. In the figure, we can observe that the magnitude of the slope of the analytic solution increases as evaporation proceeds and that our simulation matches with the analytic solution until $t = 0.9t_f$. During the last 10% of the lifetime, depinning of the contact line occurs due to large surface tension at the contact line which leads small discrepancy between simulation data and the analytic solution.

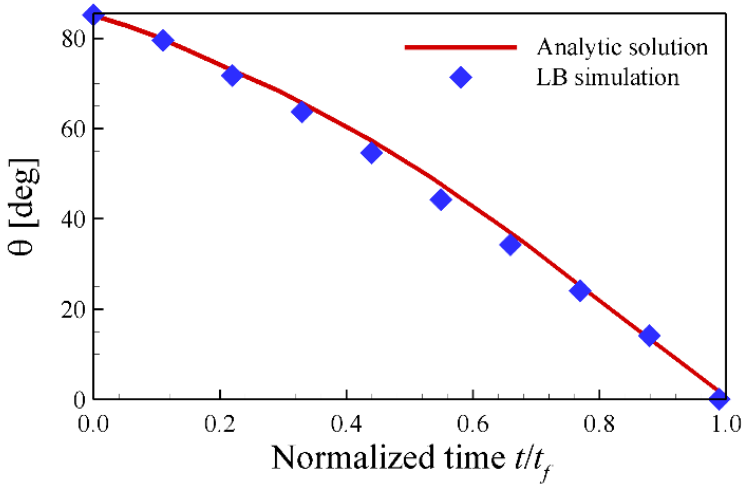

Figure 8. The evolution of the contact angle during evaporation in a constant contact radius mode is plotted as a function of normalized time t/t_f where t_f is the lifetime of the droplet in evaporation. The solid line indicates analytic solution obtained by Eq. (3.2) and the symbols correspond to the results of LB simulation.

A typical outward velocity field in a droplet during evaporation is obtained and compared with the analytical solutions. Fig. 9a and Fig. 9b illustrate the streamline and the outward flow, respectively, induced by the higher evaporation rate near the droplet edge. Especially, in Fig. 9b the flow patterns are shown that the vertical velocity components are larger than the radial velocity components while the radial velocities are dominant near the contact line.

To quantitatively compare the flow field with the analytical solution, we plot the radial and vertical velocities according to the height of the droplet. The analytic solution is obtained by Hu and Larson [16] which is based on lubrication approximation, valid for the droplet of relatively small height. For the comparison, we convert the LB units to the physical system units using the characteristic droplet radius of $1\ \mathrm{mm}$ and the time scale of evaporation, $6\ \mathrm{min}$. As shown in Fig. 10, our simulation results are consistent with the analytic solution. The simulation data of vertical velocity (Fig. 10b) shows lower consistency with the analytic solution than that of radial velocity (Fig. 10a). This discrepancy comes from the spurious current [24, 37] which is a small vortex generated near the interface. In our simulation, the magnitude of spurious current is approximately $1 \times 10^{-4}\mathrm{mm/s}$ near the interface which is comparable to the vertical velocity.

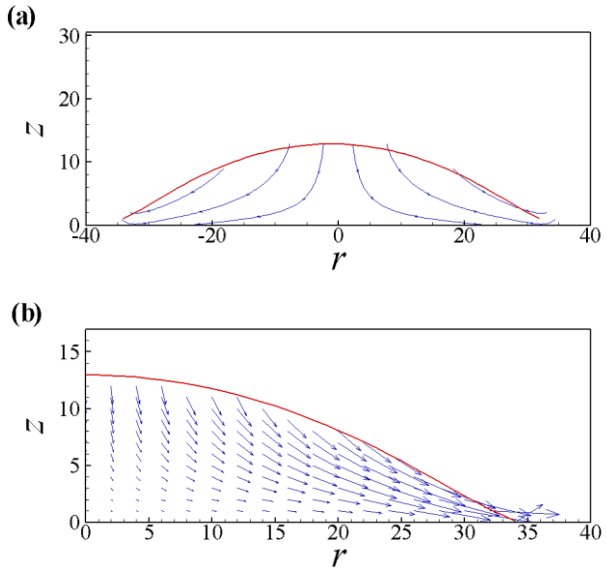

Figure 9. LB simulation results at the contact angle of 40° $(t = 0.6t_f)$. (a) Streamline and (b) vector field of the flow field for the right half of the droplet.

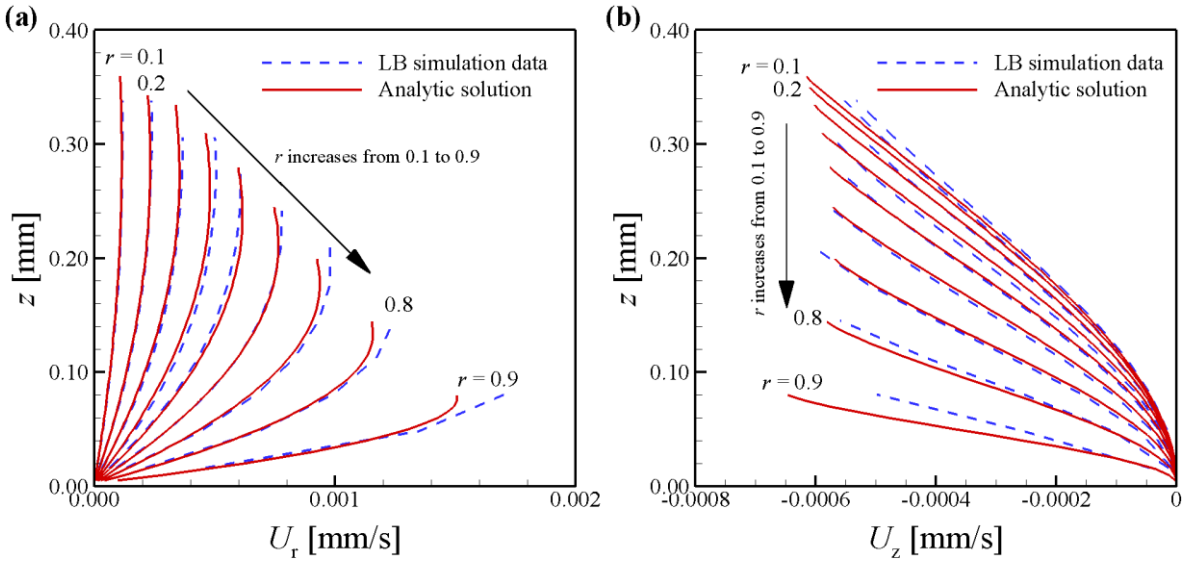

Figure 10. (a) Radial and (b) vertical velocity components according to the droplet height at 10 different radial positions from 0.1 mm to 0.9 mm at a contact angle of 40°. The solid lines correspond to the analytic solution and the dashed lines correspond to the LB solution.

3.2. Colloidal particle deposition patterns

In this section, we simulate the evaporation of a droplet containing colloids with a pinned contact line. The simulation is performed in a 2-dimensional domain, size of 301×151. During equilibration process, periodic boundary conditions are imposed at the top, left, and right boundaries and at the bottom substrate the wall boundary condition is given. The substrate is chemically patterned, where the hydrophilic ($\theta \approx 0^{\circ}$) substrate is imposed at the center and surrounded by hydrophobic ($\theta \approx 130^{\circ}$) area, similar to the schematic of Fig. 7. The initial conditions of the droplet are set as follows: the contact radius is $R_0 = 100$ with the contact angle $\theta_0 \approx 90^{\circ}$, and the densities of $\rho_{ma}^{\sigma} = \rho_{mi}^{\bar{\sigma}} = 0.7$ and $\rho_{mi}^{\sigma} = \rho_{ma}^{\bar{\sigma}} = 0.04$. The interaction parameter in Eq. (2.19) is set to $G_{\sigma\bar{\sigma}} = 2.8$. The initial density of the colloid particles is $\rho^c = 0.5$ within the droplet, and the density outside of the droplet is $\rho^c = 0.01$. After equilibration, we obtain $\rho_{ma}^{\sigma} \approx 0.64$ and $\rho_{mi}^{\sigma} \approx 0.12$ as the equilibrium densities of the fluid component σ.

To simulation the evaporation of a droplet containing colloids, we then impose evaporation boundary conditions of ρ_H at the top, left and right boundaries, and the wall boundary condition is imposed at the bottom substrate for the fluid components. The wall boundary conditions are imposed at all sides of the domain for colloidal particles.

The particle density distribution is obtained by varying the Peclet number (Pe), which is the ratio of the rate of convection to diffusion of particles. That is, the Peclet number in our simulation is defined as follows

$$Pe = \frac{R_0 v_c}{D_c}, \tag{3.5}$$

where v_c is the characteristic velocity and the diffusion coefficient for the colloid particle, D_c, is given by Eq. (2.27) in Section 2.3.1. Note that the characteristic velocity v_c depends on the evaporation rate which depends on the evaporation boundary density ρ_H. In our simulation, the characteristic velocity is varied from 0.001 to 0.003 according to the boundary density of $\rho_H = 0.07$ to 10^{-5}. In addition, we change the diffusion coefficient from 0.1 to 0.23 by changing the relaxation parameter τ^c from 0.8 to 1.2.

The density distribution of particle at the contact angle of 25° is shown in Fig. 11. In the simulation, we observed the particle deposition pattern in the vicinity of the contact line for three different Peclet numbers of $0.4, 1.6,$ and 3.

Figure 11. Particle density distribution for various Peclet numbers: (a) $Pe = 0.4$, (b) $Pe = 1.6$ and (c) $Pe = 3$.

Since diffusion dominates at the low value of Pe, the motion of the particle is primarily driven by the density gradient of the particle. This is seen in Fig. 11a, where the density distribution is relatively homogeneous at $Pe = 0.4$. As the Peclet number increases, the convective particle motion predominates, which leads particles to be accumulated near the contact line (known as the "coffee-ring" phenomenon). From Fig. 11b-c, it is readily observed that particles are more accumulated at the droplet edge and the concentration at the edge increases with increasing Pe. This increase is also shown in Fig. 12, where the density distribution is plotted for a right half of the droplet.

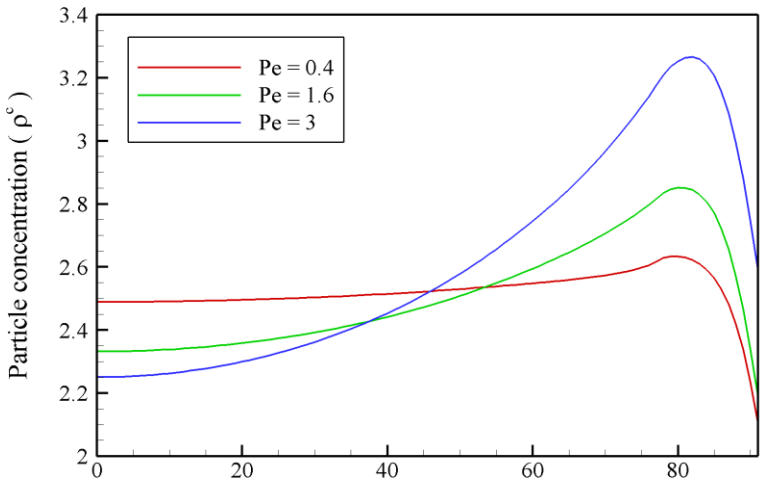

Figure 12. Deposition profiles for various Peclet numbers

3.3. Surfactant-induced Marangoni flow

In the present section, we simulate a surfactant-laden droplet evaporation using our LB surfactant model to investigate the flow filed inside the droplet, the contact line dynamics, and the shape deformation during evaporation. The simulation is performed in a 2-dimensional domain for which the domain size is 301×151. During the equilibration process, the periodic boundary conditions are given at the top, left, and right boundaries, and the wall boundary condition at the bottom substrate. The substrate is chemically patterned, where the hydrophilic ($\theta \approx 0^{\circ}$) substrate is located at the center of the domain and surrounded by hydrophobic ($\theta \approx 130^{\circ}$) area similar to the schematic of Fig. 7 in Section 3.1. The initial conditions of the droplet are set as the contact radius of $R_0 = 100$ with contact angle $\theta_0 \approx 90^{\circ}$, and the densities of $\rho_{ma}^{\sigma} = \rho_{mi}^{\bar{\sigma}} = 0.7$ and $\rho_{mi}^{\sigma} = \rho_{ma}^{\bar{\sigma}} = 0.04$. The interaction parameter in Eq. (2.9) is set to $G_{\sigma\bar{\sigma}} = 2.8$. The density of the surfactant is initialized by $\rho^s = 0.5$ within the droplet, and $\rho^s = 0.01$ outside the droplet. The parameter related to the interfacial force F_{int} in Eq. (2.30) is set to $G_{int}^{\sigma} = -5$ (attractive) between fluid component σ and the surfactant s, and $G_{int}^{\sigma} = 5$ (repulsive) between fluid component $\bar{\sigma}$ and surfactant s. The relaxation parameter for the surfactant is set to be $\tau = 0.8$ which enables the convective motion of the surfactant to be dominant.

After equilibration, the equilibrium density of the surfactant inside the droplet become $\rho^s \approx 0.503$. We then imposed evaporation boundary conditions of $\rho_H = 0$ at the top, left, and right boundaries and the wall boundary condition is imposed at the bottom substrate. The wall boundary conditions are imposed at all sides of the domain for surfactant.

Fig. 13a shows the concentration distribution at $t = 0.17t_f$. Due to the outward capillary flow, the high concentration of surfactant in the vicinity of the contact line is observed. This high concentration of surfactant at the droplet interface weakens the surface tension of the droplet. Since the surface tension is relatively higher at the droplet center where the concentration of surfactants is lower than the periphery, the surface tension gradient is formed along the droplet surface. The presence of the surface

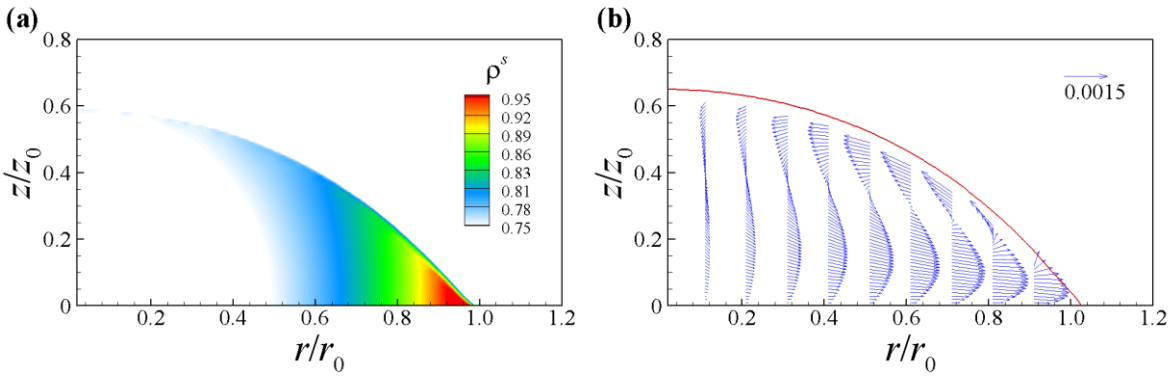

Figure 13. The concentration distribution of (a) surfactants and (b) the flow field inside the droplet at $t = 0.7t_f$

tension gradient generates the surface flow from the droplet edge toward the droplet apex (Fig. 13b). This surface flow is commonly called Marangoni flow.

Fig. 14a and b show the velocity field in the droplet at $t = 0.17t_f$ and $0.41t_f$, respectively. As evaporation proceeds, we can observe the stronger Marangoni flow in Fig. 14b compared to that in Fig. 14a and the contact line movement. The Marangoni flow induces the depinning of the contact line, moves the contact line inward, and deforms the shape of the droplet. Theoretically, from Eq. (2.18), the depinning process occurs with $\theta = \theta_A$, since l_B goes to zeros as evaporation proceeds. However, when the external force exists near the contact line, it is possible that the contact line to be receded along the hydrophilic substrate where $\theta > \theta_A$. In the simulation, the Marangoni stress acts as the external force and the depinning is found to occur at $\theta \approx 58^{\circ}$, where $\theta_A = 0^{\circ}$. As the evaporation proceeds, the large concentration gradient inside the droplet is generated due to the outward capillary flow and then the strong Marangoni flow at the interface is induced by the large concentration gradient. It is interesting to note that the strong Marangoni flow deforms the profile of the droplet in such a way that the droplet is inflated in the middle and deflated at the edge compared to the droplet in a spherical shape in the absence of the Marangoni flow (red dashed line in Fig. 14b). In the experiments conducted by Tsoumpas et al. [38] the similar inflated profile of the droplet is observed. In Fig. 14b, the profile of the droplet interface (red solid line) exhibits the maximum slope near the contact line. This indicates that the strong Marangoni flow toward the apex of the droplet delivers more liquid to the apex of the droplet causing the inflation of the droplet at the center.

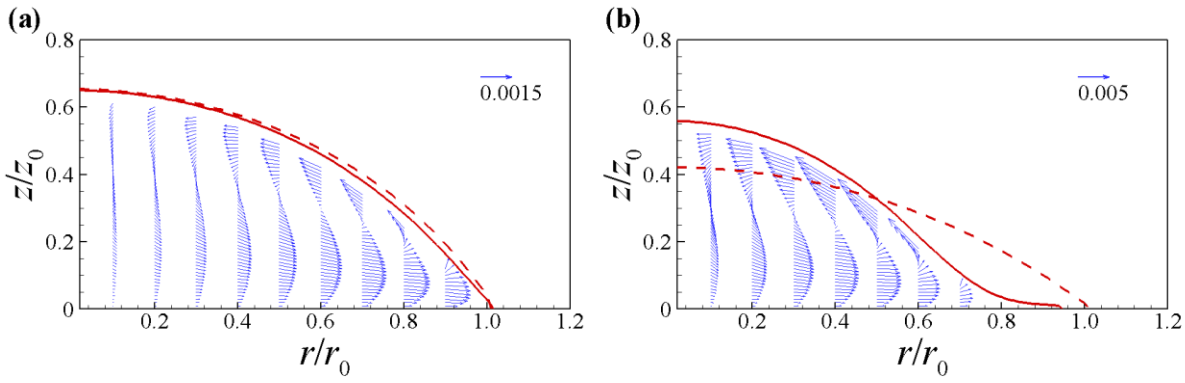

Figure 14. Time dependent flow field at (a) $t = 0.17t_f$ and (b) $t = 0.41t_f$. The red solid line indicates the profile of the droplet interface. The dashed line indicates the profile of the droplet interface without Marangoni flow. The data for the dashed line is obtained by the simulation of evaporation of a pure droplet.

4. Conclusions

In this thesis, we developed the LB model to simulate the dynamics of colloids and surfactant in an evaporating droplet with a fixed contact line. We implemented the pseudopotential lattice Boltzmann model, which is a popular method to simulate multiphase and multicomponent fluids. The evaporation is caused by the density gradient of fluid surrounding the droplet. The contact line is fixed by the local force balance. We used the chemically patterned substrate to generate the unbalanced Young's force at the hydrophobic-hydrophilic boundary of the substrate. The local Young's force at the contact line maintains the contact line to be pinned. Next, we proposed a novel LB model to simulate the movements of colloids and surfactant in a drying droplet. Using the LB model, we solve the advection-diffusion equation for both colloid and surfactant within the droplet. To retain colloids and surfactant inside the droplet during evaporation, we imposed the external force, which has a similar formulation to the interaction force in the pseudopotential lattice Boltzmann model to the particle distribution function at the interface of a droplet. The effect of surfactant on the surface tension is also incorporated in the model by using the Langmuir's isotherm, which is one of the mostly used non-linear surfactant equations of state.

The simulation results show the applicability of the novel LB model: First, we simulated the evaporation of a droplet with the fixed contact line and compared the evolutions with the analytic solutions. The flow field inside the droplet and the contact angle evolution are found to agree well with the analytical results. Second, we compared the deposition patterns in a droplet with various Peclet numbers. We show three different deposition patterns with the Peclet numbers: $Pe = 0.4, 1.6$ and 3. Since large Pe indicates the dominance of the convective motion of particles over diffusion, we observed the high concentration of colloids near the droplet edge when $Pe = 3$. Accordingly, when $Pe = 0.4$, the concentration distribution of colloids is relatively homogenous in the droplet. Finally, the model for surfactant successfully captured the contact line dynamics and the shape deformation of the surfactant-laden droplet during evaporation. We also observed the Marangoni flow which flows from the contact line to the apex of the droplet since the concentration gradient of surfactant is higher at the contact line. As the evaporation proceeds, the Marangoni flow became stronger, leading to the depinning of the contact line. After depinning, the droplet evaporates in the CA mode on the hydrophilic substrate and the inflation of the droplet shape at the center is observed. This inflation is caused by the stronger Marangoni flow toward the apex.

After the verification of the model for colloids and surfactant through the Chapman-Enskog analysis, it can be used for simulating the intricate system of a drying droplet with colloids and surfactant in unified way in context of the lattice Boltzmann simulations.

References

[1] R. D. Deegan, O. Bakajin, T. F. Dupont, G. Huber, S. R. Nagel, and T. A. Witten, "Contact line deposits in an evaporating drop," *Physical Review E,* vol. 62, no. 1, pp. 756-765, 2000.

[2] T. Furuta, M. Sakai, T. Isobe, and A. Nakajima, "Evaporation behavior of microliter- and sub-nanoliter-scale water droplets on two different fluoroalkylsilane coatings," *Langmuir,* vol. 25, no. 20, pp. 11998-2001, Oct 20 2009.

[3] J. Chen *et al.*, "Evaporation-induced assembly of quantum dots into nanorings," *ACS Nano,* vol. 3, no. 1, pp. 173-80, Jan 27 2009.

[4] T. P. Bigioni, X. M. Lin, T. T. Nguyen, E. I. Corwin, T. A. Witten, and H. M. Jaeger, "Kinetically driven self assembly of highly ordered nanoparticle monolayers," *Nat Mater,* vol. 5, no. 4, pp. 265-70, Apr 2006.

[5] M. Singh, H. M. Haverinen, P. Dhagat, and G. E. Jabbour, "Inkjet printing-process and its applications," *Adv Mater,* vol. 22, no. 6, pp. 673-85, Feb 9 2010.

[6] R. G. Picknett and R. Bexon, "The evaporation of sessile or pendant drops in still air," *Journal of Colloid and Interface Science,* vol. 61, no. 2, pp. 336-350, 1977.

[7] M. E. R. Shanahan, "Simple Theory of "Stick-Slip" Wetting Hysteresis," *Langmuir,* vol. 11, no. 3, pp. 1041-1043, 1995.

[8] F.-C. Wang and H.-A. Wu, "Pinning and depinning mechanism of the contact line during evaporation of nano-droplets sessile on textured surfaces," *Soft Matter,* vol. 9, no. 24, 2013.

[9] N. Anantharaju, M. Panchagnula, and S. Neti, "Evaporating drops on patterned surfaces: transition from pinned to moving triple line," *J Colloid Interface Sci,* vol. 337, no. 1, pp. 176-82, Sep 1 2009.

[10] D. I. Yu *et al.*, "Wetting and evaporation phenomena of water droplets on textured surfaces," *International Journal of Heat and Mass Transfer,* vol. 90, pp. 191-200, 2015.

[11] Y. C. Chuang, C. K. Chu, S. Y. Lin, and L. J. Chen, "Evaporation of water droplets on soft patterned surfaces," *Soft Matter,* vol. 10, no. 19, pp. 3394-403, May 21 2014.

[12] H. P. Jansen, H. J. W. Zandvliet, and E. S. Kooij, "Evaporation of elongated droplets on chemically stripe-patterned surfaces," *International Journal of Heat and Mass Transfer,* vol. 82, pp. 537-544, 2015.

[13] J. Zhang, F. Muller-Plathe, and F. Leroy, "Pinning of the Contact Line during Evaporation on Heterogeneous Surfaces: Slowdown or Temporary Immobilization? Insights from a Nanoscale Study," *Langmuir,* vol. 31, no. 27, pp. 7544-52, Jul 14 2015.

[14] Q. Li, P. Zhou, and H. J. Yan, "Pinning-Depinning Mechanism of the Contact Line during Evaporation on Chemically Patterned Surfaces: A Lattice Boltzmann Study," *Langmuir,* vol.

32, no. 37, pp. 9389-96, Sep 20 2016.

[15] R. D. Deegan, O. Bakajin, T. F. Dupont, G. Huber, S. R. Nagel, and T. A. Witten, "Capillary flow as the cause of ring stains from dried liquid drops," (in English), *Nature,* vol. 389, no. 6653, pp. 827-829, Oct 23 1997.

[16] H. Hu and R. G. Larson, "Analysis of the Microfluid Flow in an Evaporating Sessile Droplet," *Langmuir,* vol. 21, no. 9, pp. 3963-3971, 2005.

[17] H. Hu and R. G. Larson, "Marangoni effect reverses coffee-ring depositions," *J Phys Chem B,* vol. 110, no. 14, pp. 7090-4, Apr 13 2006.

[18] A. Marin, R. Liepelt, M. Rossi, and C. J. Kahler, "Surfactant-driven flow transitions in evaporating droplets," *Soft Matter,* vol. 12, no. 5, pp. 1593-600, Feb 7 2016.

[19] K. L. Maki and S. Kumar, "Fast evaporation of spreading droplets of colloidal suspensions," *Langmuir,* vol. 27, no. 18, pp. 11347-63, Sep 20 2011.

[20] M. Zhao and X. Yong, "Modeling Evaporation and Particle Assembly in Colloidal Droplets," *Langmuir,* vol. 33, no. 23, pp. 5734-5744, Jun 13 2017.

[21] S. Frijters, F. Günther, and J. Harting, "Effects of nanoparticles and surfactant on droplets in shear flow," *Soft Matter,* vol. 8, no. 24, 2012.

[22] X. Shan and H. Chen, "Lattice Boltzmann model for simulating flows with multiple phases and components," *Physical Review E,* vol. 47, no. 3, pp. 1815-1819, 1993.

[23] W. Zhu, M. Wang, and H. Chen, "Study on multicomponent pseudo-potential model with large density ratio and heat transfer," *International Communications in Heat and Mass Transfer,* vol. 87, pp. 183-191, 2017.

[24] X. Shan, "Analysis and reduction of the spurious current in a class of multiphase lattice Boltzmann models," *Phys Rev E Stat Nonlin Soft Matter Phys,* vol. 73, no. 4 Pt 2, p. 047701, Apr 2006.

[25] Y. H. Qian, D. D'Humières, and P. Lallemand, "Lattice BGK Models for Navier-Stokes Equation," *Europhysics Letters (EPL),* vol. 17, no. 6, pp. 479-484, 1992.

[26] X. Shan and G. Doolen, "Multicomponent lattice-Boltzmann model with interparticle interaction," *Journal of Statistical Physics,* vol. 81, no. 1-2, pp. 379-393, 1995.

[27] S. P. Dawson, S. Chen, and G. D. Doolen, "Lattice Boltzmann computations for reaction-diffusion equations," *Journal of Chemical Physics,* vol. 98, no. 2, pp. 1514-1523, 1993.

[28] R. Kumar, S. S. Nivarthi, H. T. Davis, D. M. Kroll, and R. S. Maier, "Application of the lattice-Boltzmann method to study flow and dispersion in channels with and without expansion and contraction geometry," *International Journal for Numerical Methods in Fluids,* vol. 31, no. 5, pp. 801-819, 1999.

[29] V. K. Michalis, A. N. Kalarakis, E. D. Skouras, and V. N. Burganos, "Mesoscopic modeling of flow and dispersion phenomena in fractured solids," *Computers & Mathematics With*

Applications, vol. 55, no. 7, pp. 1525-1540, 2008.

[30] D. Hessling, Q. Q. Xie, J. J. Harting, and J. J. Harting, "Diffusion dominated evaporation in multicomponent lattice Boltzmann simulations," *Journal of Chemical Physics,* vol. 146, no. 5, p. 054111, 2017.

[31] P. Yuan and L. Schaefer, "Equations of state in a lattice Boltzmann model," *Physics of Fluids,* vol. 18, p. 042101, 2006.

[32] N. Martys, N. Martys, H. Chen, and H. Chen, "Simulation of multicomponent fluids in complex three-dimensional geometries by the lattice Boltzmann method.," *Physical Review E,* vol. 53, no. 1, pp. 743-750, 1996.

[33] H. Huang, D. T. Thorne, M. G. Schaap, and M. C. Sukop, "Proposed approximation for contact angles in Shan-and-Chen-type multicomponent multiphase lattice Boltzmann models.," *Physical Review E,* vol. 76, no. 6, p. 066701, 2007.

[34] X. Shan and G. Doolen, "Diffusion in a multicomponent lattice Boltzmann equation model," *Physical Review E,* vol. 54, no. 4, pp. 3614-3620, 1996.

[35] J. Eastoe and J. S. Dalton, "Dynamic surface tension and adsorption mechanisms of surfactants at the air–water interface," *Advances in Colloid and Interface Science,* vol. 85, pp. 103-144, 2000.

[36] J. Stauber, S. Wilson, B. R. Duffy, and K. Sefiane, "Evaporation of droplets on strongly hydrophobic substrates," *Langmuir,* vol. 31, no. 12, pp. 3653-3660, 2015.

[37] K. Connington and T. Lee, "A review of spurious currents in the lattice Boltzmann method for multiphase flows," *Journal of Mechanical Science and Technology,* vol. 26, no. 12, pp. 3857-3863, 2013.

[38] Y. Tsoumpas, S. Dehaeck, A. Rednikov, and P. Colinet, "Effect of Marangoni Flows on the Shape of Thin Sessile Droplets Evaporating into Air," *Langmuir,* vol. 31, no. 49, pp. 13334-40, Dec 15 2015.

Acknowledgements

I would like to express my sincere gratitude to my advisor, Professor Chun Sang Yoo who gave me the opportunity and provided his invaluable guidance to me to do this research.

I would also like to express my special thanks to Doctor Narina Jung for providing her guidance and suggestions throughout the research.

Also, I would like to thank all member of our laboratory. All of them give me invaluable ideas which can broaden my view, and they make the best surroundings for me to adopt the life in UNIST. Every moment that I spent with them will not be forgettable.

I always thanks to my family who respect my decision to enter the graduate school. Without their untiring love and support, I would not be here.